Actomyosin-mediated cellular tension drives increased tissue stiffness and -catenin activation to induce epidermal hyperplasia and tumor growth

Cancer Cell. Author manuscript; available in PMC 2012 June 14.
Published in final edited form as:
Cancer Cell. 2011 June 14; 19(6): 776–791.
doi: 10.1016/j.ccr.2011.05.008

PMCID: PMC3115541
NIHMSID: NIHMS297093

Actomyosin-mediated cellular tension drives increased tissue stiffness and β-catenin activation to induce interfollicular epidermal hyperplasia and tumor growth

Michael S Samuel,[1,6] Jose I Lopez,[2] Ewan J McGhee,[1] Daniel R Croft,[1] David Strachan,[1] Paul Timpson,[1] June Munro,[1] Ewald Schröder,[3] Jing Zhou,[4] Valerie G Brunton,[4] Nick Barker,[5] Hans Clevers,[5] Owen J Sansom,[1] Kurt I Anderson,[1] Valerie M Weaver,[2] and Michael F Olson[1,7]

[1] Beatson Institute for Cancer Research, Glasgow G61 1BD, UK
[2] Department of Surgery, UCSF, San Francisco, CA 94143, USA
[3] Cancer Research Technology, WIBR, London WC1E 6BT, UK
[4] Edinburgh Cancer Research Centre, Edinburgh EH4 2X9, UK
[5] Hubrecht Institute, Uppsalalaan 8, 3584CT Utrecht, Netherlands
[7] Corresponding author: MF Olson, Tel: +44 141 330 3654, Email: m.olson@beatson.gla.ac.uk
[6] Present address: Centre for Cancer Biology, Frome Road, Adelaide 5000, Australia

SUMMARY

Tumors and associated stroma manifest mechanical properties that promote cancer. Mechanosensation of tissue stiffness activates the Rho/ROCK pathway to increase actomyosin-mediated cellular tension to re-establish force equilibrium. To determine how actomyosin tension affects tissue homeostasis and tumor development, we expressed conditionally-active ROCK2 in mouse skin. ROCK activation elevated tissue stiffness via increased collagen. β-catenin, a key element of mechanotranscription pathways, was stabilized by ROCK activation leading to nuclear accumulation, transcriptional activation and consequent hyperproliferation and skin thickening. Inhibiting actomyosin contractility by blocking LIMK or myosin ATPase attenuated these responses, as did FAK inhibition. Tumor number, growth and progression were increased by ROCK activation, while ROCK blockade was inhibitory, implicating actomyosin-mediated cellular tension and consequent collagen deposition as significant tumor promoters.

Introduction

Tumors grow in complex environments in which external factors, such as tissue rheology (Butcher et al., 2009), influence growth and progression. Despite the association of tissue stiffness with cancer being so well established that palpation and elastography are diagnostic procedures for some tumors, the mechanisms that translate mechanosensation of external conditions to the induction of tumor-promoting responses remain poorly understood.

Rho GTPases act as network hubs that transduce signals from the extracellular environment to proteins that mediate biological responses (Parsons et al., 2010). ROCK1 and ROCK2 are essential for RhoA and RhoC-initiated actomyosin contractility through phosphorylation of substrates including LIM kinases (LIMK), myosin regulatory light chains (MLC2) and the myosin-binding subunit of the MLC phosphatase (MYPT), which facilitates cell movement and contributes to cancer metastasis (Olson and Sahai, 2009). Rho activation was first found after growth factor receptor stimulation (Ridley and Hall, 1992), but Rho proteins respond to additional inputs, including external force, to affect cytoskeletal structure and function (Parsons et al., 2010). External tensile force results in compensatory Rho/ROCK activation, to increase cellular tension and reestablish force equilibrium (Wozniak et al., 2003; Zhao et al., 2007). At the same time, internal cellular tension remains in equilibrium with the external microenvironment through the reorganization, modification and/or synthesis of extracellular matrix (ECM) proteins (Chiquet et al., 2009; Wu et al., 2007). In some pathological contexts, force equilibration may not be achieved, resulting in a mechanical autocrine loop that drives rheological changes and consequent tissue stiffness.

Skin is a mechanically responsive tissue (Silver et al., 2003), which forms a barrier that protects against damaging environmental stresses. Net tension in the skin is a balance between external collagen fibrils and internal actomyosin cellular tension (Silver et al., 2003). To maintain barrier integrity, cells are constantly renewed in a tightly controlled process termed epidermal homeostasis (Blanpain and Fuchs, 2009). Squamous cell carcinoma (SCC) develops in keratinocytes that have differentiated and moved from the basal layer, and is the second most common skin cancer (Xie, 2008). Rho and ROCK signaling are associated with SCC (Jiang et al., 2010; Lefort et al., 2007; Wang et al., 2009), although details of how Rho/ROCK may promote SCC are lacking.

In this current study, we investigated how actomyosin cellular tension influences tissue rheology, epidermal homeostasis and tumor growth and progression.

Results

ROCK activation increases tissue stiffness

To investigate how cellular tension affects tissue homeostasis and cancer, we created K14-ROCK:ER mice (Samuel et al., 2009a) that express a chimeric protein (ROCK:ER) consisting of the human ROCK2 kinase domain fused to mutant 17β-estradiol-insensitive estrogen receptor (ER) hormone binding domain (HBD) (Littlewood et al., 1995) and enhanced green fluorescent protein (EGFP) under the control of the K14 promoter (Figures S1A, B). Upon HBD binding of tamoxifen or 4-hydroxytamoxifen (4HT), ROCK:ER is activated and phosphorylates physiological substrates leading to actomyosin-mediated contractility (Samuel et al., 2009a). K14-ROCK:ER and a control kinase-dead (KD) version (K14-KD:ER) were each targeted to the *Hprt* locus, leading to expression ~15% of endogenous ROCK2 (Samuel et al., 2009a). Consistent with previous results (Samuel et al., 2009a), 4HT treatment of K14-ROCK:ER mouse skin increased Mlc2 phosphorylation, but not in K14-KD:ER or Wild-type (WT) control mice (Figure 1A). Thr696 phosphorylation of the myosin binding subunit of the Mlc phosphatase (pMypt1), which inhibits Mlc dephosphorylation (Feng et al., 1999), was also increased by 4HT specifically in K14-ROCK:ER mouse skin (Figure 1A).

To determine how ROCK activation and consequent cellular tension affected tissue rheology, K14-ROCK:ER and WT skin dorsal skin was given 5 daily 4HT treatments, then subjected to rheological analysis by atomic force microscopy (AFM). Compared to WT skin, ROCK activated skin showed an AFM force map skewed towards high kPa values and significant increase in Young's modulus,

demonstrating increased tissue stiffness (Figure 1B, C). When viewed through orthogonal polarizing filters, ROCK activated skin also had increased picrosirius red fluorescence, indicating increased collagen fiber diameters (Figure 1B, C). Accordingly, second harmonic generation (SHG) analysis of 4HT treated K14-ROCK:ER skin showed increased collagen density and expanded distribution from the epidermal surface to greater depths compared to WT (Figures 1D, E, Movies S1, S2 and S3), confirming previous reports of correlations between optical and mechanical properties of collagen *in vivo* (Raub et al., 2010; Raub et al., 2008). These results show that ROCK-induced actomyosin cellular tension is associated with increased collagen fiber diameter and elevated collagen deposition over a broader distribution. Therefore, internal cellular tension drives significant tissue-level compensatory responses.

ROCK activation drives epidermal proliferation and skin thickening

Within 5 days of daily 4HT treatment, ROCK activated skin was significantly thicker than K14-KD:ER and WT skin (Figure 2A, S2A), associated with interfollicular epidermal expansion by several cell layers. ROCK-induced epidermal thickening was associated with a significant doubling in BrdU-positive proliferating basal keratinocytes relative to control K14-KD:ER or WT mice (Figure 2B, S2B). K14-ROCK:ER keratinocytes cultured in 4HT grew in soft agar, yielding 2.5-fold as many anchorage-independent colonies as K14-KD:ER keratinocytes (Figure 2C). Y27632 treatment abolished this effect, showing ROCK dependence of the increased anchorage-independent growth.

ROCK-induced skin thickening was associated with expansion of the suprabasal interfollicular epidermal cell layer expressing cytokeratin 1 (K1) and ectopic expression of the follicular cytokeratin 6 (K6) by immunofluorescence and FACS analyses (Figure 2D, S2B, S2C). K14-KD:ER and WT control mice had no skin thickening and retained normal K1 and K6 expression following 4HT treatment (Figure 2D, S2D). Inhibition of lysyl oxidase (Lox) with β-aminopropionitrile (BAPN) to reduce collagen fibril cross-linking in rigid matrices (Levental et al., 2009) reversed K6 induction (Figure 2D). K6 expression, which is commonly observed in SCC (Haass et al., 2006; Khayyata et al., 2009), has been associated with either epidermal hyperplasia or inflammation (Kopan and Fuchs, 1989; Stoler et al., 1988; Weiss et al., 1984). However, inflammatory infiltrate as observed in DMBA/TPA papillomas was not evident in ROCK activated skin (Figure S2E). The observations that ROCK activation caused skin thickening, increased proliferation, K6 expression and anchorage independent growth indicate that sustained actomyosin-mediated cellular tension has a pro-proliferative role within the epidermis.

ROCK activates β-catenin and elevates transcriptional target expression

β-catenin has important roles in epidermal homeostasis and tumorigenesis, regulating progenitor cell proliferation through Tcf/Lef target gene transcription (Lo Celso et al., 2004; Malanchi et al., 2008; Nguyen et al., 2009; Zhu and Watt, 1999). β-catenin is also a central element in transcription pathways responsive to mechanical stimulation (Arnsdorf et al., 2009; Sen et al., 2009), suggesting that β-catenin might mediate responses to elevated collagen and tissue stiffness. ROCK activation within the epidermis caused significant increases in expression of the Tcf/Lef target genes CD44 (Wielenga et al., 1999), Cyclin D1 (Shtutman et al., 1999; Tetsu and McCormick, 1999) and Lgr5 (Jaks et al., 2008) at mRNA and protein levels (Figure 3A, 3B, 3C) relative to K14-KD:ER and WT epidermis. CD44 and Cyclin D1 mRNA were also upregulated in primary cultured keratinocytes by ROCK activation (Figure S3).

To confirm Tcf/Lef transcriptional activation, K14-ROCK:ER and K14-KD:ER mice were crossed with TOPGAL reporter mice, which express β-galactosidase under the control of an engineered TOP promoter containing 3 tandem Tcf/Lef consensus binding sites, (DasGupta and Fuchs, 1999). TOPGAL; K14-ROCK:ER mice expressed β-galactosidase throughout the interfollicular epidermis upon 4HT

treatment, unlike TOPGAL; K14-KD:ER mice (Figure 3D). Luciferase-based Tcf/Lef (TOPFlash) assays of cultured primary keratinocytes also showed significant 4HT-induced Tcf/Lef transcriptional activity in ROCK:ER expressing cells, comparable to KD:ER or ROCK:ER cells treated with GSK3β inhibitor 6-bromoindirubin-39-oxime (BIO) (Meijer et al., 2004) (Figure 3E). These results show that ROCK activation increased β-catenin transcriptional activity and target gene transcription, which could drive interfollicular epidermal cell proliferation.

Immunofluorescence of ROCK-activated epidermis revealed re-distribution of β-catenin (red fluorescence and red trace) from membrane to cytoplasm (red arrowheads) and nucleus (blue arrowheads), compared to identically treated control K14-KD:ER mice (Figure 4A, B). In contrast, E-cadherin (green fluorescence and green trace), which associates with β-catenin in adherens junctions remained at the cell membrane (Figure 4A, B). An image processing macro (see Supplemental Experimental Procedures) developed to quantify nuclear and cytoplasmic localization of β-catenin immunofluorescence showed ~2-fold increase in nuclear β-catenin upon ROCK activation and 5-fold elevation in total β-catenin relative to K14-KD:ER epidermis, consistent with β-catenin western blots of epidermal lysates (Figure 4C). β-catenin positive cells were also found increased in ROCK-activated epidermis by FACS analysis of dissociated cells (Figure 4D). Immunofluorescence of ROCK-activated epidermis using an antibody against activated β-catenin (dephosphorylated at Ser37 and Thr41) (van Noort et al., 2002) revealed that nuclear localized β-catenin is the activated form (Figure 4E), which was associated with increased phosphorylation of GSK3β on Ser9 that blocks phosphorylation of substrate such as β-catenin (Dajani et al., 2001). BAPN treatment to inhibit Lox activity and collagen cross-linking reversed both the nuclear accumulation of active β-catenin and GSK3β phosphorylation (Figure 4E). These results indicate that the epidermal hyperproliferation in ROCK-activated epidermis is associated with Tcf/Lef transcriptional activity brought about by stabilization and activation of β-catenin.

β-catenin deletion abolishes ROCK-induced epidermal hyperproliferation

To determine whether β-catenin mediates ROCK-induced hyperproliferation, we crossed K14-ROCK:ER and K14-KD:ER mice onto a background homozygous for a conditional floxed β-catenin allele ($Ctnnb1^{tm2Kem}$) (Brault et al., 2001) and K14-driven Cre recombinase/ER fusion protein expression (K14-Cre:ER) (Vasioukhin et al., 1999). K14-ROCK:ER; β-$catenin^{Fl/Fl}$; K14-Cre:ER compound mutant mice treated for 5 days with 4HT exhibited loss of β-catenin within the interfollicular epidermis (Figure 5A, S4A), which did not affect ROCK activation or LIMK activity, as shown by Mypt and cofilin phosphorylation respectively (Figure S4B). β-catenin deletion blocked ROCK-induction of CD44v3-v10 or Cyclin D1 (Figure 5B, S4C). In the absence of β-catenin, ROCK activation did not induce epidermal hyperproliferation as indicated by reduced Ki67 immunoreactivity or skin thickening (Figure 5C, S4D). Indeed, β-catenin loss completely abolished ROCK-mediated skin thickening (Figure 5D) and normalized Ki67 labeling (Figure 5E), but did not affect ROCK-induced collagen deposition (Figure 5F), indicating that elevated collagen is not a consequence of β-catenin activation. β-catenin loss had no effect on epidermal homeostasis in control K14-KD:ER mice (Figure S4E). Consistent with β-catenin being a driver of epidermal proliferation, K14-Cre:ER, $Ctnnb1^{tm1Mmt/+}$ mice expressing a 4HT-inducible version of constitutively active β-catenin (Harada et al., 1999) exhibited ~5-fold interfollicular epidermal thickening associated with increased β-catenin (Figure 5G). These results indicate that ROCK induced interfollicular epidermal hyperproliferation is β-catenin dependent, associated with increased β-catenin transcriptional activity and expression of β-catenin regulated transcriptional targets, placing ROCK activation and actomyosin-mediated cellular tension in a pathway leading to β-catenin activation.

Actomyosin contractility is required for ROCK-induced epidermal proliferation

LIMK1 and LIMK2 are phosphorylated and activated by ROCK, and in turn phosphorylate and inactivate the F-actin severing cofilin proteins (Scott and Olson, 2007). To determine whether inhibiting mediators of actomyosin contractility would block ROCK induced epidermal hyperproliferation, a selective and non-toxic LIMK inhibitor (LIMKi; compound 3 in (Ross-Macdonald et al., 2008)), was applied in combination with 4HT. Staining with phospho-cofilin specific antibody (Figure S5A) revealed that a single LIMKi treatment abolished cofilin phosphorylation (Figure S5B). LIMKi application with 4HT for 5 days blocked skin thickening and ectopic interfollicular K6 in K14-ROCK:ER mice (Figure 6A white arrows, Figure 6B, S5C), accompanied by absence of cofilin phosphorylation (Figure 6A, Figure S5C) and reduced β-catenin levels (Figure 6A yellow arrow). Similarly, inhibition of myosin ATPase activity to block actomyosin contraction with daily Blebbistatin (Straight et al., 2003) application eliminated skin thickening, ectopic interfollicular K6 expression and reduced β-catenin levels (Figure 6A, B). Lox inhibition with BAPN to reduce collagen cross-linking also significantly reduced skin thickening (Figure 6B). LIMKi and Blebbistatin also reduced ROCK-induced BrdU incorporation in 4HT treated K14-ROCK:ER skin to a level comparable to untreated K14-ROCK:ER skin (Figure 6C), confirming that ROCK-induced hyperproliferation was reversed by inhibition of actomyosin contractility. In primary cultured keratinocytes, Y27632 or LIMKi reduced ROCK-induced BrdU incorporation to levels observed in untreated cells or 4HT treated control K14-KD:ER keratinocytes (Figure S5D). ROCK induced collagen deposition also was significantly reduced by LIMKi or Blebbistatin (Figure 6D). These observations indicate that interfollicular epidermal hyperproliferation, β-catenin accumulation and collagen deposition following ROCK activation is dependent upon sustained cellular tension mediated by actomyosin contractility.

β-catenin stabilization induced by integrin-responsive signaling pathway

Collagen is a major extracellular matrix protein that influences cellular behaviors by promoting integrin clustering and activating downstream signaling (Egeblad et al., 2010), with FAK activation being an early response (Zhao and Guan, 2009). FAK autophosphorylation at Tyr397 was elevated in 4HT treated ROCK:ER skin relative to control KD:ER or WT skin (Figure 7A), while application of the selective FAK inhibitor PF-562271 (Roberts et al., 2008) blocked FAK autophosphorylation (Figure 7A). The PI3K/Akt axis has been shown to be important in FAK-mediated signaling downstream of collagen-activated integrins (Tian et al., 2002). Akt phosphorylation on an activating Ser473 position was elevated in ROCK-activated skin and reduced by topical application of FAK inhibitor PF-562271 (Figure 7B). Akt phosphorylates GSK3β on Ser9, thereby creating a competitive pseudosubstrate that blocks substrate phosphorylation (Dajani et al., 2001). ROCK activation increased GSK3β Ser9 phosphorylation relative to control 4HT-treated WT or KD:ER skin (Figure 7C), accompanied by decreased β-catenin phosphorylation on GSK3β sites Ser37 and Thr41 (Figure 7C). Both increased inhibitory GSK3β inhibitory Ser9phosphorylation and decreased β-catenin Ser37 and Thr41 phosphorylation were reversed by FAK inhibitor PF562271 (Figure 7C). In support of a FAK > PI3K/AKT > GSK3β pathway being responsible for β-catenin regulation, the increased levels of β-catenin and skin thickening in ROCK activated skin were blocked by FAK inhibitor PF562271 (Figure 7D, 7E).

ROCK promotes papillomagenesis

To test the effect of cellular tension on tumor growth and progression, we examined how ROCK-activation influenced skin tumors in a 2-stage chemical carcinogenesis protocol. Syngeneic papillomas are induced in FVB/N mice by one application of the mutagen dimethylbenz[a]anthracene (DMBA)

followed by repeated applications of 12-O-tetradecanoylphorbol-13-acetate (TPA) (Hennings et al., 1993). Papillomas arise and reproducibly convert at low frequency to invasive carcinomas by a mechanism involving H-Ras mutations and MAP-kinase activation (Balmain et al., 1984; Quintanilla et al., 1986). Tumors produced by this procedure model human SCC and have been used to determine the dependence on genes such as beta;-catenin (Malanchi et al., 2008).

K14-ROCK:ER or K14-KD:ER mouse cohorts backcrossed at least 10 generations onto the FVB/N background were treated twice weekly with vehicle or 4HT in addition to DMBA/TPA for a total of 15 weeks (Figure 8A), at which point carcinomas were observed and the experiment halted. Significantly increased papillomas were observed in 4HT-treated K14-ROCK:ER mice compared to 4HT or vehicle-treated K14-KD:ER mice or vehicle-treated K14-ROCK:ER mice (Figures 8B, S6A). A shift towards larger papillomas (Figure 8C) and increased papilloma incidence (Figure 8B) resulted in a significantly greater total papilloma burden (a function of papilloma volume and number) in 4HT-treated K14-ROCK:ER mice relative to vehicle-treated control and to both K14-KD:ER treatment groups (Figure 8D). Only the ROCK-activated cohort had papilloma to carcinomas conversion within 15 weeks (Figure 8D). SHG analysis of epidermal collagen revealed significantly higher levels in the keratinocyte layer associated with resident papillomas (Figure 8E). Total and nuclear β-catenin were significantly increased in 4HT treated K14-ROCK:ER papillomas compared to 4HT treated K14-KDK:ER papillomas, consistent with the increased tumor growth (Figure 8F, S6B). These results show that sustained ROCK activation is sufficient to elevate collagen, activate β-catenin and increase papilloma incidence, growth and progression to carcinoma.

The selective ROCK inhibitor Y27632 (Uehata et al., 1997) was used to reduce Rock signaling during DMBA/TPA-induced papillomagenesis. Y27632 treatment of DMBA/TPA treated FVB/N mice markedly reduced pMypt levels within hyperproliferative skin and papillomas (Figure S6C), confirming tissue penetration and Rock inhibition. Pure FVB/N cohorts treated with Y27632 (Figure 8G) twice weekly during the DMBA/TPA procedure developed significantly fewer (Figures 8H, S6C) and smaller papillomas (Figure 8I) than control vehicle treated mice, resulting in significantly reduced tumor burden (Figure 8J). Papilloma to carcinoma conversion rate was 6.5% was in the DMBA/TPA-treated cohort, but only 1.5% in the cohort co-administered Y27632 within the 20 week treatment course (Figure 8J). Collagen levels were significantly reduced in the keratinocyte layer associated with resident papillomas as determined by SHG (Figure 8K). Y27632 treated papillomas also exhibited significantly lower Cyclin D1 and Ki67 histoscores compared to vehicle treated papillomas (Figure S6D). Total as well as nuclear β-catenin was significantly reduced in Y27632 treated papillomas, consistent with the reduced tumor growth (Figure 8L, S6E). These results show that Rock inhibition lowered epidermal collagen, reduced papillomagenesis and delayed tumor growth and progression by reducing proliferation, indicating that actomyosin-mediated cellular tension makes crucial contributions to tumor promotion.

Human skin tumors exhibit elevated ROCK expression and activity

To determine whether ROCK signaling was altered in human skin cancers, immunohistochemical analysis of a tissue microarray derived from 40 cases of human squamous skin carcinomas was carried out with a pan-specific ROCK1/2 antibody (Figure S6F) and a phospho-specific antibody for the ROCK substrate MYPT as an indicator of ROCK activation. Most skin tumors analyzed (90%) expressed high ROCK levels relative to phenotypically normal skin (Table S1, Figure S6G). Positive pixel analysis of SCC samples revealed statistically significant increases in ROCK and pMYPT relative to normal skin samples (Figure 8M), and MYPT phosphorylation correlated significantly with ROCK expression (

Figure 8N). These results show that ROCK over-expression correlates with ROCK activation and is a common occurrence in human SCC, suggesting that ROCK activation drives cellular tension to promote human skin cancer. However, pMYPT staining indirectly correlates with MLC2 phosphorylation and actomyosin contractility and as a consequence, inferences should be treated with some caution.

Discussion

Collagen, a major component of the extracellular matrix, may be increased in density as well as in post-translational modifications that alter the structure and organization of collagen fibers, contributing to variations in tissue stiffness (Egeblad et al., 2010). Cells grown *in vitro* on stiff collagen matrices have been shown to activate Rho and ROCK signaling leading to increased actomyosin contractility, which generates counter-balancing cellular tension in an attempt to balance internal and external forces (Paszek et al., 2005; Wozniak et al., 2003) in a process dubbed “mechanoreciprocity” (Butcher et al., 2009). In addition to this outside>inside signaling, there is evidence from cell-based experiments that ROCK-mediated actomyosin contractility inside the cell may, conversely, reorganize extracellular matrix structures or stimulate increased matrix protein synthesis and secretion (Butcher et al., 2009; Discher et al., 2005; Huang and Ingber, 2005; Provenzano et al., 2008; Wozniak et al., 2003).

We now show that the conditional-activation of ROCK, the principal driver of actomyosin contractility and cellular tension *via* MYPT and MLC phosphorylation (Figure 1A) (Samuel et al., 2009a), in murine epidermis results in significant modification of the extracellular matrix through increased collagen deposition leading to increased tissue stiffness. Accompanying the increased tissue stiffness, activation of the mechanically-responsive β-catenin transcriptional co-activator promotes target gene transcription and increased epidermal cell proliferation. These results show that the development of cellular tension profoundly affects the external microenvironment and influences tissue homeostasis.

It has long been observed that tumor development is associated with increased tissue stiffness. In fact, cancers such as mammary tumors are often detected by palpation or elastography of the abnormally rigid tissue that surrounds them. Increased stiffness of the cellular microenvironment contributes significantly to tumor cell survival, proliferation and progression (Egeblad et al., 2010). During the course of tumor growth and progression, the tissue microenvironment undergoes significant remodeling, which increases the mechanical forces that cancer cells are subjected to evoking compensatory responses *via* Rho and ROCK activation (Butcher et al., 2009). Results from the present study also show that this relationship is reciprocal; increased ROCK-induced cellular tension *in vivo* causes alterations in the extracellular matrix and increased tissue stiffness. An important question is whether the increased tissue stiffness induced by elevated cellular tension is sufficient to promote tumor growth and progression. The results from our study show that conditional ROCK activation and consequent increase in collagen deposition did indeed increase tumor growth and progression, while ROCK inhibition reduced these responses. Therefore, in addition to external tissue-level forces modulating cellular responses, mechanical alterations at the cellular-level can influence tissue mechanoproperties that promote cancer. It has generally been assumed that the increased Rho and ROCK activity commonly observed in cancer cells reflects a role in promoting invasion and metastasis (Olson and Sahai, 2009). However, results from this study indicate that altered expression and/or activity of actomyosin regulators may promote tumor growth by influencing the tumor microenvironment. Therefore, in addition to ROCK inhibition, targeting proteins such as LIMK and myosin that work downstream of ROCK in the regulation of the actomyosin cytoskeleton may have anti-tumor therapeutic benefits by counteracting the effects of cellular tension on the microenvironment. While our studies clearly show a role of actomyosin contractility in generating increased tissue stiffness

via collagen deposition, further work will be required to determine the relative contributions of tumor and tumor-associated cells such as stromal fibroblasts.

Mechanical regulation of β-catenin has been well documented in bone, a tissue often subjected to continuous and repeated strain. Here, mechanical factors lead to β-catenin stabilization and nuclear translocation, which is associated with the activation of a FAK > PI3K/Akt > GSK3β phosphorylation cascade (Case and Rubin, 2010; Santos et al., 2010), in agreement with the observations in mouse skin. Mechanical activation of the *Drosophila* β-catenin homologue armadillo as a result of tissue-level forces has also been reported (Desprat et al., 2008). Increased β-catenin levels and concentration in cytoplasmic/nuclear compartments have been reported in human cutaneous SCC tumors (Malanchi et al., 2008; Papadavid et al., 2002), consistent with the results in hyperproliferative murine skin (Figure 4). Interestingly, nuclear β-catenin levels are often elevated at the host-tumor interface of invasive colorectal carcinomas (Brabletz et al., 2005). These areas would be predicted sites of elevated mechanoresistance leading to increased external forces and consequently sites of high compensatory Rho/ROCK activation. It would also follow that, in contrast to hard-wired genetic or epigenetic alterations, these relatively acute mechanical responses to external tension contribute to the transdifferentiation potential of tumor cells and promote adaptability of tumors to continuously evolving microenvironmental factors, for instance during the process of metastasis.

EXPERIMENTAL PROCEDURES

Cell Culture

Primary keratinocytes were extracted from tail skin as described (McLean et al., 2001). Cells were maintained at 37°C/5% CO_2/3% O_2, in keratinocyte growth medium (KBM-2; Clonetics) with epidermal growth factor (10 ng/ml), insulin (5 μg/ml), hydrocortisone (0.5 μg/ml), bovine pituitary extract protein (70 μg/ml) and 50 μM Ca^{2+} on collagen-1 coated dishes (Becton Dickinson).

Clonogenic survival assays

Primary keratinocytes were seeded on dishes coated with 0.9% agarose/DMEM (containing 10% FBS, L-glutamine and antibiotics) at 2×10^4 cells/well in DMEM containing 0.45% agarose ± 1 μM 4HT and maintained at 37 °C/10% CO_2. DMEM±1 μM 4HT was added to each well twice weekly. Two weeks post-seeding, colonies >80 μm in diameter were scored from 5 fields/well.

Human Tissue Microarrays

Human TMAs were purchased from Protein Biotechnologies, which confirms that all tissue samples were collected under strict IRB approved guidelines/protocols with informed consent. All collected human tissues were treated under strict confidentiality and according to appropriate applicable laws that protect the confidentiality of personal information. No names or any other identity information were revealed during the development of tissue arrays, nor to end users, and as a result are exempt from consideration by the Beatson Institute Committee on Human Subjects in Medical Research due to being anonymized and non-traceable. CRUK guidelines were followed in the handling and analysis of this material. TMAs containing tumor tissue and normal cores from 40 cases of squamous skin cancer were baked for two hours at 60°C prior to immunohistochemistry.

Mice

K14-ROCK:ER mice were described previously (Samuel et al., 2009a). TOPGAL [Tg(Fos-lacZ)34Efu/J] mice were from Jackson Labs. All procedures were performed under appropriate licenses and according

to the UK Home Office guidelines.

In vivo gene induction and/or activation and enzyme inhibition

4-hydroxytamoxifen (4HT, Sigma, 1mg) in ethanol (100 μl) was applied to shaved dorsal skin and repeated daily for up to 30 days. Inhibitors (per mouse, Blebbistatin–23μg; Y27632–25μg; LIMKi–32μg; PF-562271–160μg; BAPN–760μg) were applied topically once daily for 5 consecutive days in appropriate vehicle.

Keratinocyte extraction for western and FACS

Epidermal tissue was separated as previously described (Nowak and Fuchs, 2009). Epidermal cells were lysed in 1 × RIPA buffer for western analysis, Trizol (Invitrogen) for mRNA extraction or fixed in 4% paraformaldehyde for FACS analysis using standard methods. All FACS analyses were carried out by first gating K14 positive cells.

Chemical carcinogenesis

Chemical carcinogenesis was carried out as described (Quintanilla et al., 1986). DMBA (Sigma, 25 μg) in acetone (150 μl) was applied directly to shaved dorsal skin. After three days, TPA (Sigma, 6.25 μg) was applied in acetone (150 μl) and repeated twice weekly for 20 weeks or until a carcinoma developed. Papillomas were counted and measured weekly. Final papilloma burden was calculated by summing the individual products of papilloma number and the square of each papilloma diameter, which was then normalized across cohorts against the K14-KD:ER average. Carcinoma conversion rate was calculated as percentage of carcinomas observed relative to total number of papillomas.

Histology and immunohistochemistry

Histology and immunohistochemistry were performed as described (Samuel et al., 2009b). Antigen retrieval buffer and antibody dilutions used appear in Supplemental Experimental Procedures. Slides were imaged using a Hamamatsu Nanozoomer NDP slide scanner (Hamamatsu Photonics) and Digital Slide Server (Slidepath) software.

Elastic Modulus Measurements and collagen staining

The mechanical properties of fresh frozen skin (Foutz et al., 1992) were assayed using an MFP3D-Bio inverted optical AFM mounted on a Nikon TE2000-U inverted phase microscope (Asylum Research). Pyramidal Si_3N_4 cantilevers with a manufacturer spring constant of 0.06N/m fitted with 5 μm borosilicate glass microspheres (Novascan Tech) were calibrated using the thermal noise method (Hutter and Bechhoefer, 1993) prior to AFM indentation. Force maps were acquired by sample indentation with a force of 5nN. The Hertz model of impact (Hertz, 1881) was used to calculate the Young's elastic modulus of resulting force curves. Heat maps were generated using Igor Pro 6 (Wavemetrics). Picrosirius Red staining was carried out as described (Levental et al., 2009; Paszek et al., 2005).

Acquisition of second harmonic generation (SHG) data from collagen

Samples of depilated and freshly excised skin were imaged using a 20× 0.95 NA water immersion objective on an inverted Nikon TE-2000 microscope body. The excitation source was a Ti:Sapphire femto-second laser cavity (Coherent Chameleon Ultra II), coupled into a LaVision Biotec Trim-scope scan-head. 890 nm excitation wavelength was used to simultaneously collect SHG signal (435±20 nm) from collagen and auto-fluorescence (525±25 nm) from surrounding tissue. Signal was acquired from

three separate volumes measuring 500 × 500 × 200 μm across each sample, in steps of 2 μm imaging depth, with an acquisition time of 30 minutes per volume.

Analysis of SHG signal from collagen

ImageJ was used to calculate percentage area covered by SHG signal per optical slice within a volume, after conversion to a binary image based upon a manually determined threshold value. Results were expressed as median ± SEM across all data sets for each genotype. A Grey Level Contrast Matrix (GLCM) analysis was performed upon optical slices at which maximum coverage was observed for each phenotype using the USB GLCM plug-in for ImageJ. The shown parameters were calculated for varying pixel displacement values. Results were expressed as average ± SEM for each parameter for all genotypes.

Statistical analysis

Unless indicated, statistical significance was determined by Student's *t*-test. Data are shown as means ± SD unless indicated. Box and whisker plots show medians and quartiles with p-values calculated using Mann-Whitney test for comparing medians. In all cases, $p<0.05$ was used as significance cut-off.

Supplementary Material

01

02

03

04

Acknowledgments

We acknowledge the support of the Think Pink breast cancer group who funded purchase of the NDP slide scanner. Thanks to Martin Stockley for LIMKi synthesis. Funding for this study was from Cancer Research UK (MFO), IRACDA Scholars in Science K12GM081266 award (JIL), W81XWH-05-1-0330 from the DOD BCRP and CA138818-01A1 from the NCI (VMW).

Footnotes

References

1. Arnsdorf EJ, Tummala P, Jacobs CR. Non-canonical Wnt signaling and N-cadherin related beta-catenin signaling play a role in mechanically induced osteogenic cell fate. PLoS One. 2009;4:e5388. [PMCID: PMC2670536] [PubMed: 19401766]
2. Balmain A, Ramsden M, Bowden GT, Smith J. Activation of the mouse cellular Harvey-ras gene in chemically induced benign skin papillomas. Nature. 1984;307:658–660. [PubMed: 6694757]
3. Blanpain C, Fuchs E. Epidermal homeostasis: a balancing act of stem cells in the skin. Nat Rev

Mol Cell Biol. 2009;10:207–217. [PMCID: PMC2760218] [PubMed: 19209183]
4. Brabletz T, Hlubek F, Spaderna S, Schmalhofer O, Hiendlmeyer E, Jung A, Kirchner T. Invasion and metastasis in colorectal cancer: epithelial-mesenchymal transition, mesenchymal-epithelial transition, stem cells and beta-catenin. Cells Tissues Organs. 2005;179:56–65. [PubMed: 15942193]
5. Brault V, Moore R, Kutsch S, Ishibashi M, Rowitch DH, McMahon AP, Sommer L, Boussadia O, Kemler R. Inactivation of the beta-catenin gene by Wnt1-Cre-mediated deletion results in dramatic brain malformation and failure of craniofacial development. Development. 2001;128:1253–1264. [PubMed: 11262227]
6. Butcher DT, Alliston T, Weaver VM. A tense situation: forcing tumour progression. Nat Rev Cancer. 2009;9:108–122. [PMCID: PMC2649117] [PubMed: 19165226]
7. Case N, Rubin J. Beta-catenin--a supporting role in the skeleton. J Cell Biochem. 2010;110:545–553. [PubMed: 20512915]
8. Chiquet M, Gelman L, Lutz R, Maier S. From mechanotransduction to extracellular matrix gene expression in fibroblasts. Biochimica et Biophysica Acta (BBA) - Molecular Cell Research. 2009;1793:911–920.
9. Dajani R, Fraser E, Roe SM, Young N, Good V, Dale TC, Pearl LH. Crystal Structure of Glycogen Synthase Kinase 3[beta]: Structural Basis for Phosphate-Primed Substrate Specificity and Autoinhibition. Cell. 2001;105:721–732. [PubMed: 11440715]
10. DasGupta R, Fuchs E. Multiple roles for activated LEF/TCF transcription complexes during hair follicle development and differentiation. Development. 1999;126:4557–4568. [PubMed: 10498690]
11. Desprat N, Supatto W, Pouille PA, Beaurepaire E, Farge E. Tissue deformation modulates twist expression to determine anterior midgut differentiation in Drosophila embryos. Dev Cell. 2008;15:470–477. [PubMed: 18804441]
12. Discher DE, Janmey P, Wang YL. Tissue cells feel and respond to the stiffness of their substrate. Science. 2005;310:1139–1143. [PubMed: 16293750]
13. Egeblad M, Rasch MG, Weaver VM. Dynamic interplay between the collagen scaffold and tumor evolution. Curr Opin Cell Biol. 2010;22:697–706. [PMCID: PMC2948601] [PubMed: 20822891]
14. Feng J, Ito M, Ichikawa K, Isaka N, Nishikawa M, Hartshorne DJ, Nakano T. Inhibitory phosphorylation site for Rho-associated kinase on smooth muscle myosin phosphatase. J Biol Chem. 1999;274:37385–37390. [PubMed: 10601309]
15. Foutz TL, Stone EA, Abrams CF., Jr Effects of freezing on mechanical properties of rat skin. Am J Vet Res. 1992;53:788–792. [PubMed: 1524309]
16. Haass NK, Wladykowski E, Kief S, Moll I, Brandner JM. Differential Induction of Connexins 26 and 30 in Skin Tumors and Their Adjacent Epidermis. J Histochem Cytochem. 2006;54:171–182. [PubMed: 16046668]
17. Harada N, Tamai Y, Ishikawa T, Sauer B, Takaku K, Oshima M, Taketo MM. Intestinal polyposis in mice with a dominant stable mutation of the beta-catenin gene. Embo J. 1999;18:5931–5942. [PMCID: PMC1171659] [PubMed: 10545105]
18. Hennings H, Glick AB, Lowry DT, Krsmanovic LS, Sly LM, Yuspa SH. FVB/N mice: an inbred strain sensitive to the chemical induction of squamous cell carcinomas in the skin. Carcinogenesis. 1993;14:2353–2358. [PubMed: 8242866]
19. Hertz H. On the Contact of Elastic Solids. Journal für die reine und angewandte Mathematik. 1881;92:156–171.
20. Huang S, Ingber DE. Cell tension, matrix mechanics, and cancer development. Cancer Cell.

2005;8:175–176. [PubMed: 16169461]
21. Hutter JL, Bechhoefer J. Calibration of atomic-force microscope tips. Review of Scientific Instruments. 1993;64:1868–1873.
22. Jaks V, Barker N, Kasper M, van Es JH, Snippert HJ, Clevers H, Toftgard R. Lgr5 marks cycling, yet long-lived, hair follicle stem cells. Nat Genet. 2008;40:1291–1299. [PubMed: 18849992]
23. Jiang L, Liu X, Kolokythas A, Yu J, Wang A, Heidbreder CE, Shi F, Zhou X. Downregulation of the Rho GTPase signaling pathway is involved in the microRNA-138-mediated inhibition of cell migration and invasion in tongue squamous cell carcinoma. Int J Cancer. 2010;127:505–512. [PMCID: PMC2885137] [PubMed: 20232393]
24. Khayyata S, Yun S, Pasha T, Jian B, McGrath C, Yu G, Gupta P, Baloch Z. Value of P63 and CK5/6 in distinguishing squamous cell carcinoma from adenocarcinoma in lung fine-needle aspiration specimens. Diagn Cytopathol. 2009;37:178–183. [PubMed: 19170169]
25. Kopan R, Fuchs E. The use of retinoic acid to probe the relation between hyperproliferation-associated keratins and cell proliferation in normal and malignant epidermal cells. J Cell Biol. 1989;109:295–307. [PMCID: PMC2115483] [PubMed: 2473080]
26. Lefort K, Mandinova A, Ostano P, Kolev V, Calpini V, Kolfschoten I, Devgan V, Lieb J, Raffoul W, Hohl D, et al. Notch1 is a p53 target gene involved in human keratinocyte tumor suppression through negative regulation of ROCK1/2 and MRCKalpha kinases. Genes Dev. 2007;21:562–577. [PMCID: PMC1820898] [PubMed: 17344417]
27. Levental KR, Yu H, Kass L, Lakins JN, Egeblad M, Erler JT, Fong SF, Csiszar K, Giaccia A, Weninger W, et al. Matrix crosslinking forces tumor progression by enhancing integrin signaling. Cell. 2009;139:891–906. [PMCID: PMC2788004] [PubMed: 19931152]
28. Littlewood TD, Hancock DC, Danielian PS, Parker MG, Evan GI. A modified oestrogen receptor ligand-binding domain as an improved switch for the regulation of heterologous proteins. Nucleic Acids Res. 1995;23:1686–1690. [PMCID: PMC306922] [PubMed: 7784172]
29. Lo Celso C, Prowse DM, Watt FM. Transient activation of beta-catenin signalling in adult mouse epidermis is sufficient to induce new hair follicles but continuous activation is required to maintain hair follicle tumours. Development. 2004;131:1787–1799. [PubMed: 15084463]
30. Malanchi I, Peinado H, Kassen D, Hussenet T, Metzger D, Chambon P, Huber M, Hohl D, Cano A, Birchmeier W, Huelsken J. Cutaneous cancer stem cell maintenance is dependent on beta-catenin signalling. Nature. 2008;452:650–653. [PubMed: 18385740]
31. McLean GW, Brown K, Arbuckle MI, Wyke AW, Pikkarainen T, Ruoslahti E, Frame MC. Decreased focal adhesion kinase suppresses papilloma formation during experimental mouse skin carcinogenesis. Cancer Res. 2001;61:8385–8389. [PubMed: 11731413]
32. Meijer L, Flajolet M, Greengard P. Pharmacological inhibitors of glycogen synthase kinase 3. Trends Pharmacol Sci. 2004;25:471–480. [PubMed: 15559249]
33. Nguyen H, Merrill BJ, Polak L, Nikolova M, Rendl M, Shaver TM, Pasolli HA, Fuchs E. Tcf3 and Tcf4 are essential for long-term homeostasis of skin epithelia. Nat Genet. 2009;41:1068–1075. [PMCID: PMC2792754] [PubMed: 19718027]
34. Nowak JA, Fuchs E. Isolation and culture of epithelial stem cells. Methods Mol Biol. 2009;482:215–232. [PMCID: PMC2760227] [PubMed: 19089359]
35. Olson MF, Sahai E. The actin cytoskeleton in cancer cell motility. Clin Exp Metastasis. 2009;26:273–287. [PubMed: 18498004]
36. Papadavid E, Pignatelli M, Zakynthinos S, Krausz T, Chu AC. Abnormal immunoreactivity of the E-cadherin/catenin (α-, β-, and γ-) complex in premalignant and malignant non-melanocytic skin tumours. The Journal of Pathology. 2002;196:154–162. [PubMed: 11793366]

37. Parsons JT, Horwitz AR, Schwartz MA. Cell adhesion: integrating cytoskeletal dynamics and cellular tension. Nat Rev Mol Cell Biol. 2010;11:633–643. [PMCID: PMC2992881] [PubMed: 20729930]
38. Paszek MJ, Zahir N, Johnson KR, Lakins JN, Rozenberg GI, Gefen A, Reinhart-King CA, Margulies SS, Dembo M, Boettiger D, et al. Tensional homeostasis and the malignant phenotype. Cancer Cell. 2005;8:241–254. [PubMed: 16169468]
39. Provenzano PP, Inman DR, Eliceiri KW, Trier SM, Keely PJ. Contact guidance mediated three-dimensional cell migration is regulated by Rho/ROCK-dependent matrix reorganization. Biophys J. 2008;95:5374–5384. [PMCID: PMC2586586] [PubMed: 18775961]
40. Quintanilla M, Brown K, Ramsden M, Balmain A. Carcinogen-specific mutation and amplification of Ha-ras during mouse skin carcinogenesis. Nature. 1986;322:78–80. [PubMed: 3014349]
41. Raub CB, Mahon S, Narula N, Tromberg BJ, Brenner M, George SC. Linking optics and mechanics in an in vivo model of airway fibrosis and epithelial injury. J Biomed Opt. 2010;15:015004. [PMCID: PMC2844131] [PubMed: 20210444]
42. Raub CB, Unruh J, Suresh V, Krasieva T, Lindmo T, Gratton E, Tromberg BJ, George SC. Image correlation spectroscopy of multiphoton images correlates with collagen mechanical properties. Biophys J. 2008;94:2361–2373. [PMCID: PMC2257909] [PubMed: 18065452]
43. Ridley AJ, Hall A. The small GTP-binding protein rho regulates the assembly of focal adhesions and actin stress fibers in response to growth factors. Cell. 1992;70:389–399. [PubMed: 1643657]
44. Roberts WG, Ung E, Whalen P, Cooper B, Hulford C, Autry C, Richter D, Emerson E, Lin J, Kath J, et al. Antitumor activity and pharmacology of a selective focal adhesion kinase inhibitor, PF-562,271. Cancer Res. 2008;68:1935–1944. [PubMed: 18339875]
45. Ross-Macdonald P, de Silva H, Guo Q, Xiao H, Hung CY, Penhallow B, Markwalder J, He L, Attar RM, Lin TA, et al. Identification of a nonkinase target mediating cytotoxicity of novel kinase inhibitors. Mol Cancer Ther. 2008;7:3490–3498. [PubMed: 19001433]
46. Samuel MS, Munro J, Bryson S, Forrow S, Stevenson D, Olson MF. Tissue selective expression of conditionally-regulated ROCK by gene targeting to a defined locus. Genesis. 2009a;47:440–446. [PubMed: 19391117]
47. Samuel MS, Suzuki H, Buchert M, Putoczki TL, Tebbutt NC, Lundgren-May T, Christou A, Inglese M, Toyota M, Heath JK, et al. Elevated Dnmt3a activity promotes polyposis in Apc(Min) mice by relaxing extracellular restraints on Wnt signaling. Gastroenterology. 2009b;137:902–913. [PubMed: 19454286]
48. Santos A, Bakker AD, Zandieh-Doulabi B, de Blieck-Hogervorst JM, Klein-Nulend J. Early activation of the beta-catenin pathway in osteocytes is mediated by nitric oxide, phosphatidyl inositol-3 kinase/Akt, and focal adhesion kinase. Biochem Biophys Res Commun. 2010;391:364–369. [PubMed: 19913504]
49. Scott RW, Olson MF. LIM kinases: function, regulation and association with human disease. J Mol Med. 2007;85:555–568. [PubMed: 17294230]
50. Sen B, Styner M, Xie Z, Case N, Rubin CT, Rubin J. Mechanical loading regulates NFATc1 and beta-catenin signaling through a GSK3beta control node. J Biol Chem. 2009;284:34607–34617. [PMCID: PMC2787323] [PubMed: 19840939]
51. Shtutman M, Zhurinsky J, Simcha I, Albanese C, D'Amico M, Pestell R, Ben-Ze'ev A. The cyclin D1 gene is a target of the beta-catenin/LEF-1 pathway. Proc Natl Acad Sci U S A. 1999;96:5522–5527. [PMCID: PMC21892] [PubMed: 10318916]
52. Silver FH, Siperko LM, Seehra GP. Mechanobiology of force transduction in dermal tissue. Skin

Research and Technology. 2003;9:3–23. [PubMed: 12535279]
53. Stoler A, Kopan R, Duvic M, Fuchs E. Use of monospecific antisera and cRNA probes to localize the major changes in keratin expression during normal and abnormal epidermal differentiation. J Cell Biol. 1988;107:427–446. [PMCID: PMC2115222] [PubMed: 2458356]
54. Straight AF, Cheung A, Limouze J, Chen I, Westwood NJ, Sellers JR, Mitchison TJ. Dissecting Temporal and Spatial Control of Cytokinesis with a Myosin II Inhibitor. Science. 2003;299:1743–1747. [PubMed: 12637748]
55. Tetsu O, McCormick F. Beta-catenin regulates expression of cyclin D1 in colon carcinoma cells. Nature. 1999;398:422–426. [PubMed: 10201372]
56. Tian B, Lessan K, Kahm J, Kleidon J, Henke C. beta 1 integrin regulates fibroblast viability during collagen matrix contraction through a phosphatidylinositol 3-kinase/Akt/protein kinase B signaling pathway. J Biol Chem. 2002;277:24667–24675. [PubMed: 11986332]
57. Uehata M, Ishizaki T, Satoh H, Ono T, Kawahara T, Morishita T, Tamakawa H, Yamagami K, Inui J, Maekawa M, Narumiya S. Calcium sensitization of smooth muscle mediated by a Rho-associated protein kinase in hypertension. Nature. 1997;389:990–994. [PubMed: 9353125]
58. van Noort M, Meeldijk J, van der Zee R, Destree O, Clevers H. Wnt Signaling Controls the Phosphorylation Status of β-Catenin. Journal of Biological Chemistry. 2002;277:17901–17905. [PubMed: 11834740]
59. Vasioukhin V, Degenstein L, Wise B, Fuchs E. The magical touch: genome targeting in epidermal stem cells induced by tamoxifen application to mouse skin. Proc Natl Acad Sci U S A. 1999;96:8551–8556. [PMCID: PMC17554] [PubMed: 10411913]
60. Wang L, Xue L, Yan H, Li J, Lu Y. Effects of ROCK inhibitor, Y-27632, on adhesion and mobility in esophageal squamous cell cancer cells. Mol Biol Rep. 2009;37:1971–1977. [PubMed: 19649725]
61. Weiss RA, Eichner R, Sun TT. Monoclonal antibody analysis of keratin expression in epidermal diseases: a 48- and 56-kdalton keratin as molecular markers for hyperproliferative keratinocytes. J Cell Biol. 1984;98:1397–1406. [PMCID: PMC2113245] [PubMed: 6201492]
62. Wielenga VJ, Smits R, Korinek V, Smit L, Kielman M, Fodde R, Clevers H, Pals ST. Expression of CD44 in Apc and Tcf mutant mice implies regulation by the WNT pathway. Am J Pathol. 1999;154:515–523. [PMCID: PMC1850011] [PubMed: 10027409]
63. Wozniak MA, Desai R, Solski PA, Der CJ, Keely PJ. ROCK-generated contractility regulates breast epithelial cell differentiation in response to the physical properties of a three-dimensional collagen matrix. J Cell Biol. 2003;163:583–595. [PMCID: PMC2173660] [PubMed: 14610060]
64. Wu M, Wu ZF, Merajver SD. Rho proteins and cell-matrix interactions in cancer. Cells Tissues Organs. 2007;185:100–103. [PubMed: 17587814]
65. Xie J. Molecular biology of basal and squamous cell carcinomas. Adv Exp Med Biol. 2008;624:241–251. [PubMed: 18348461]
66. Zhao J, Guan JL. Signal transduction by focal adhesion kinase in cancer. Cancer Metastasis Rev. 2009;28:35–49. [PubMed: 19169797]
67. Zhao XH, Laschinger C, Arora P, Szaszi K, Kapus A, McCulloch CA. Force activates smooth muscle alpha-actin promoter activity through the Rho signaling pathway. J Cell Sci. 2007;120:1801–1809. [PubMed: 17456553]
68. Zhu AJ, Watt FM. beta-catenin signalling modulates proliferative potential of human epidermal keratinocytes independently of intercellular adhesion. Development. 1999;126:2285–2298. [PubMed: 10207152]

Figures and Tables

Figure 1

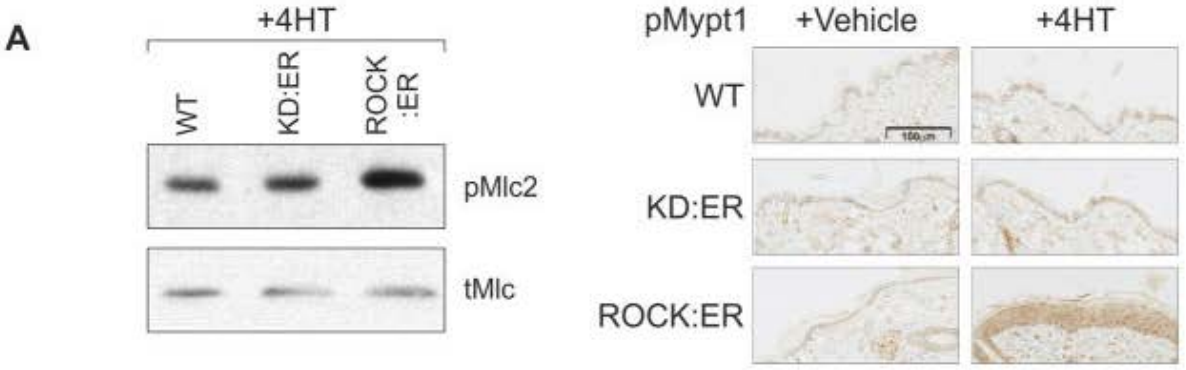

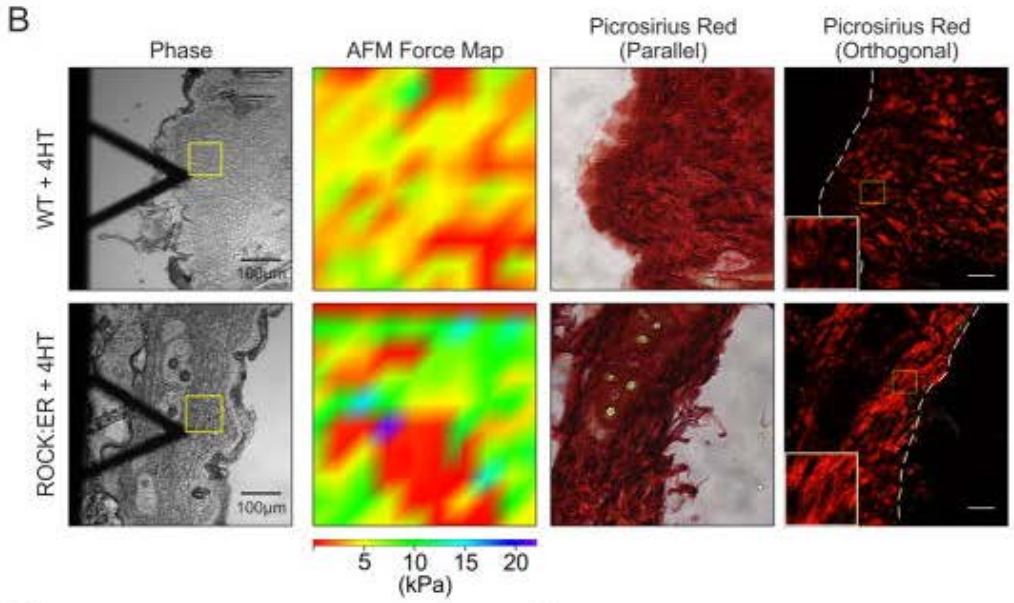

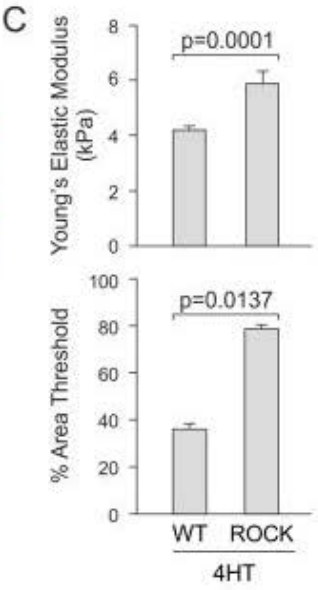

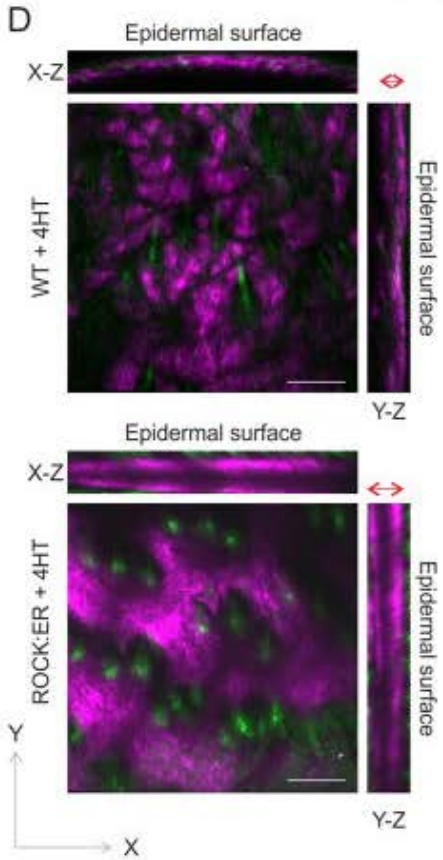

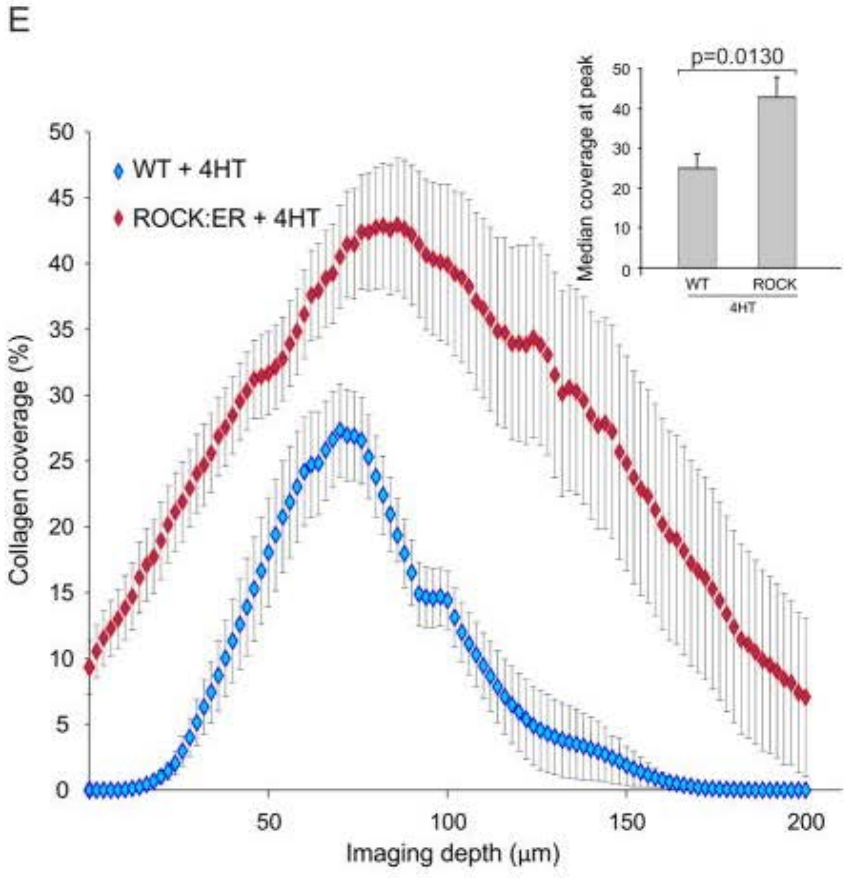

ROCK activation increases epidermal tissue stiffness and the density and depth of collagen deposition within the skin

(A) Western blot shows Mlc2 Ser19phosphorylation in 4HT treated WT, KD:ER and ROCK:ER keratinocytes. Immunohistochemical analyses show pMypt1 staining in 4HT or Vehicle treated WT, KD:ER and ROCK:ER skin.

(B) AFM Force maps of 4HT treated WT and ROCK:ER skin areas enclosed by yellow square as well as picrosirius red staining viewed through parallel or orthogonally polarizing filters.

(C) Quantification of Young's elastic Modulus and % area threshold of collagen in 4HT treated WT and ROCK:ER skin.

(D) Maximum projections along three axes of SHG collagen signal from representative 500 μm × 500 μm × 200 μm volumes of 4HT treated WT and ROCK:ER skin. Red double headed arrows show relative thicknesses of collagen layer in 4HT treated WT and ROCK:ER skin.

(E) Graphs of collagen coverage values derived from SHG signal by depth (line graph) and at peak value (histogram inset), measured over three tissue volumes each from three mice per cohort. Results are mean ± SEM.

Scale bars, 100μm

See also Figure S1 and Movies S1, S2 and S3.

Figure 2

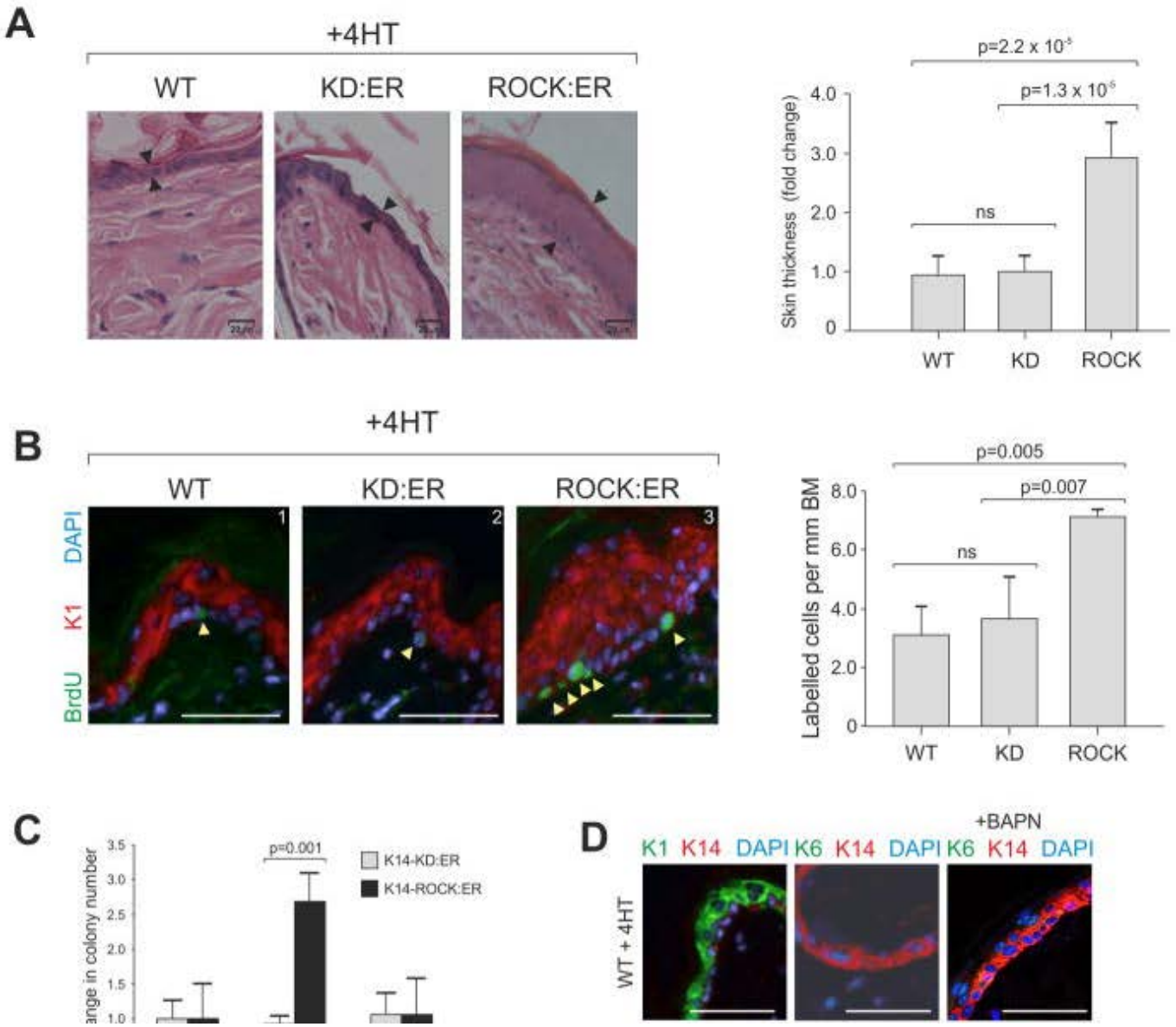

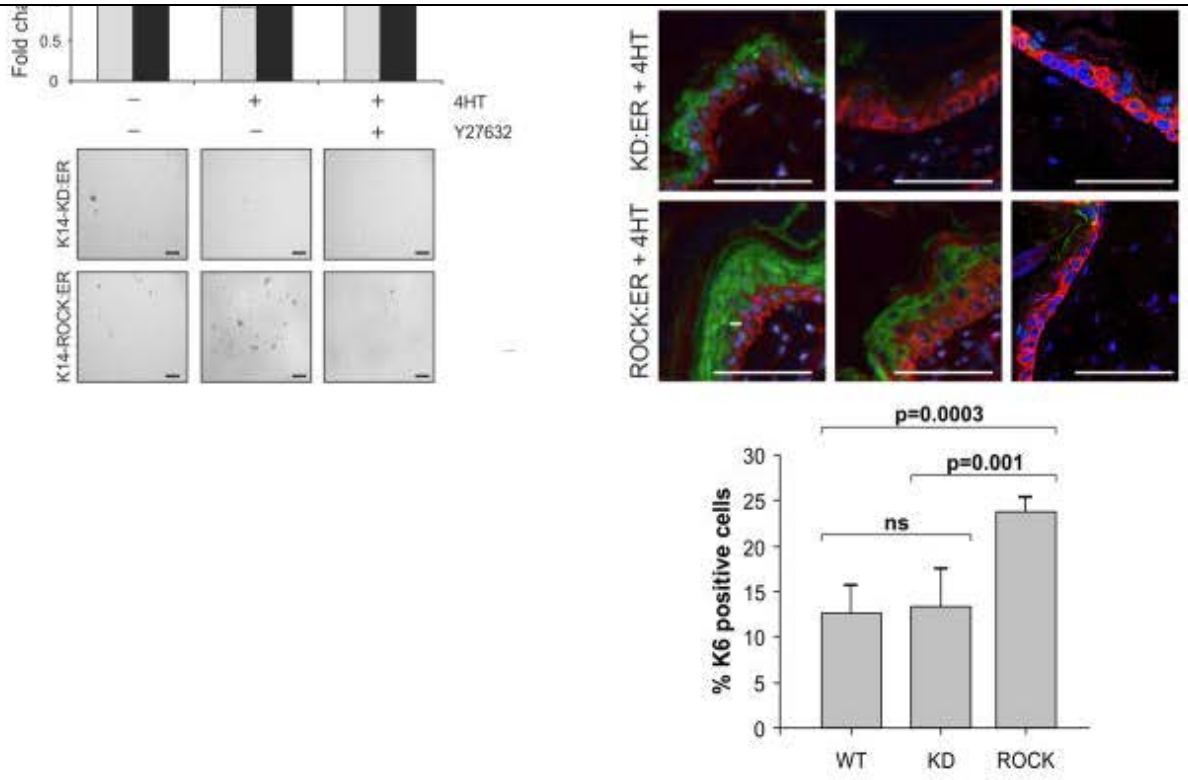

ROCK activation within murine skin causes epidermal hyperplasia

(A) Hemotoxylin and eosin (H&E) stained skin sections derived from 4HT-treated WT, KD:ER and ROCK:ER mice. Change in ROCK:ER interfollicular epidermis thickness (arrows) compared to WT and KD:ER skin following five daily topical 4HT treatments is shown in histogram. Measurements were made over five fields with three measurements taken per field. Scale bars, 20μm

(B) BrdU incorporation in skin sections derived from 4HT-treated WT, KD:ER and ROCK:ER mice. Histogram shows number of BrdU-labeled cells per mm basement membrane (BM) following 4HT treatment. Scale bars, 50 μm.

(C) Histogram shows fold change in number of colonies formed in soft agar by 4HT-treated ROCK:ER keratinocytes relative to KD:ER keratinocytes. Representative fields of colonies are shown. Scale bars, 100 μm.

(D) K1, K6 and K14 expression in skin sections derived from 4HT-treated WT, KD:ER and ROCK:ER mice, without or with BAPN treatment to inhibit lysyl oxidase. Scale bars, 100μm. Histogram shows percentage K6 positive cells within epidermis derived from 4HT-treated WT, KD:ER and ROCK:ER mice as measured by FACS (See Figure S2C for profiles).

See also Figure S2

Figure 3

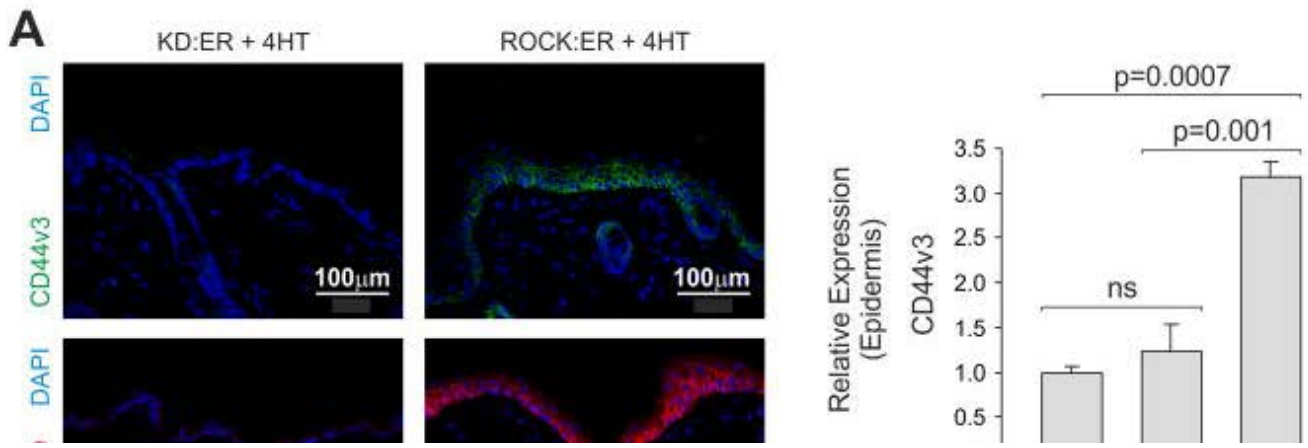

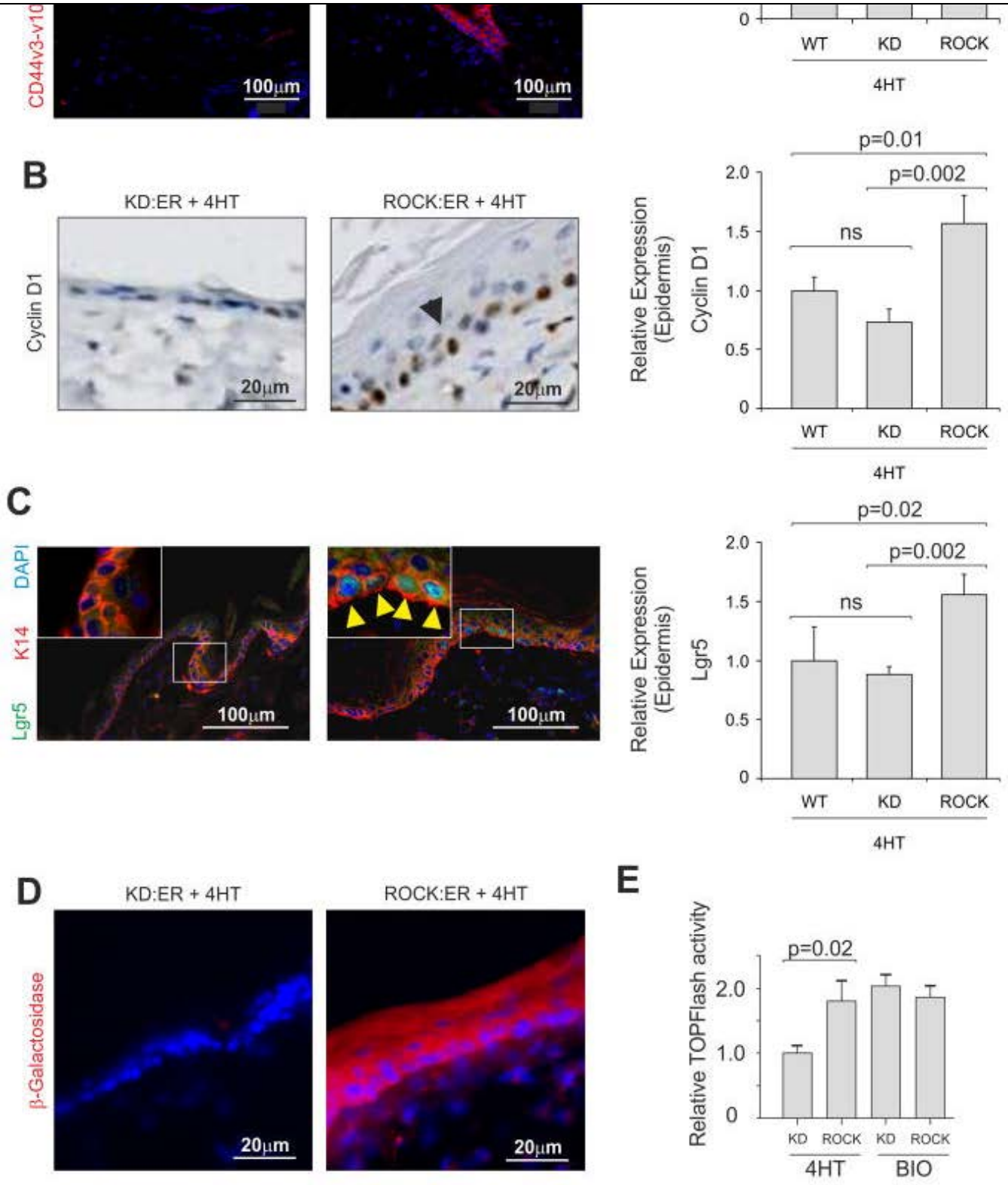

ROCK activation in the murine epidermis is associated with Tcf/Lef target gene activation

(A) Expression of CD44 variants v3 and v3-v10 in 4HT-treated KD:ER and ROCK:ER skin by immunofluorescence. Scale bars indicate 100 μm. Histogram shows CD44v3 mRNA expression within WT, KD:ER and ROCK:ER epidermis.

(B) Cyclin D1 expression in 4HT-treated ROCK:ER (arrow) and KD:ER skin. Histogram shows Cyclin D1 mRNA expression within WT, KD:ER and ROCK:ER epidermis.

(C) Ectopic expression (yellow arrows) of Lgr5 promoter-driven EGFP:Cre within interfollicular epidermis in 4HT-treated KD:ER and ROCK:ER skin. Boxed areas are enlarged in insets. Histogram shows Lgr5 mRNA expression within

WT, KD:ER and ROCK:ER epidermis.

(D) Fresh-frozen skin from 4HT-treated TOPGAL mice on KD:ER and ROCK:ER backgrounds in which β-Galactosidase activity was visualized using fluorescein di-galactoside. A red filter has been added to monochromatic channel to aid visualization.

(E) Tcf/Lef transcriptional activity in *ex vivo* cultured KD:ER and ROCK:ER keratinocytes assayed using TOPFlash reporter assay. GSK3β inhibitor BIO was used as positive control.

See also Figure S3

Figure 4

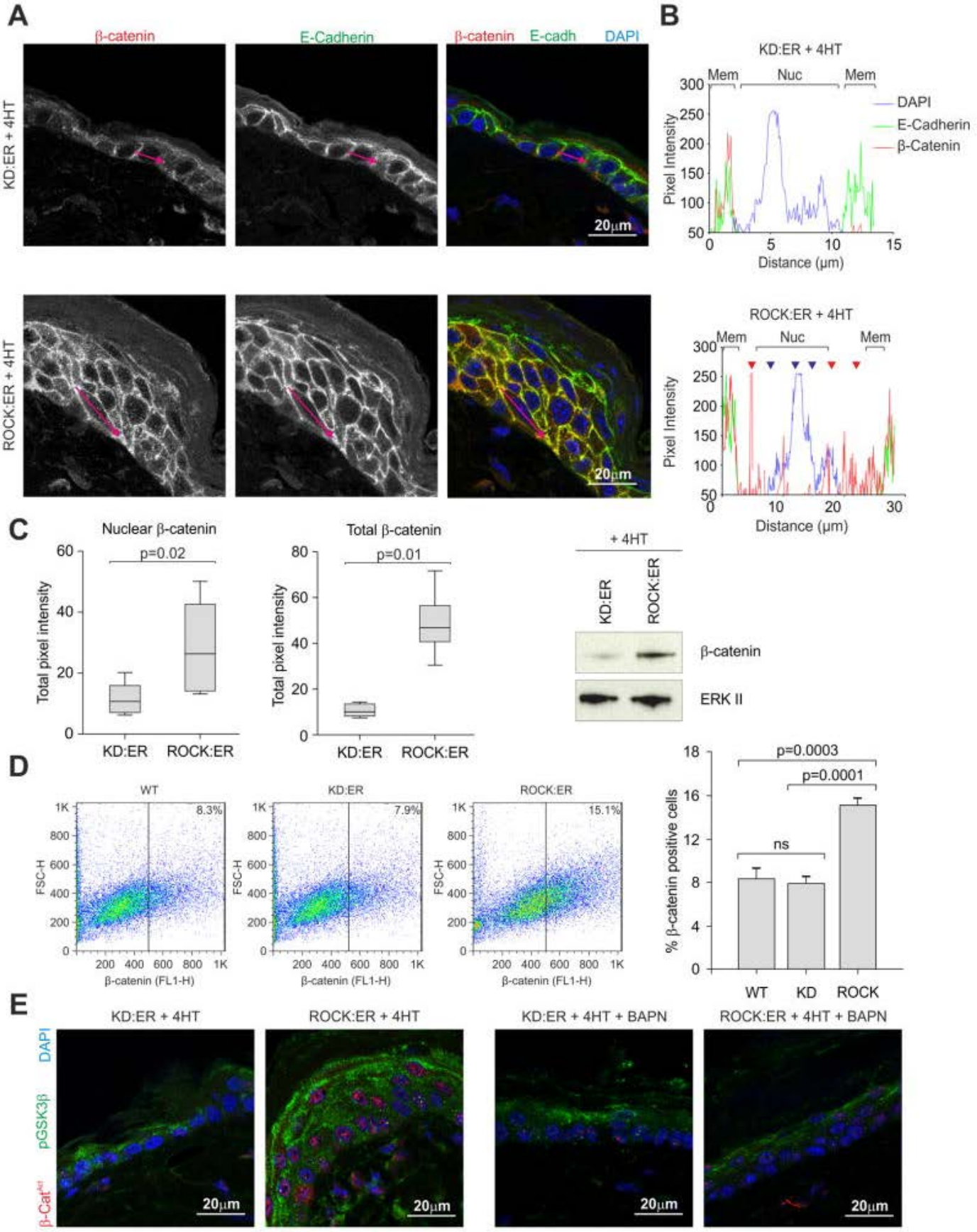

β-catenin is stabilized and relocalized upon ROCK induction within the interfollicular epidermis

(A) Confocal slice showing β-catenin (red) and E-cadherin (green) distribution in 4HT-treated KD:ER and ROCK:ER skin.

(B) Pixel intensity of red (β-catenin), green (E-cadherin) and blue (DAPI) fluorescence measured along red arrows in Figure 4A to assess co-localization. Membrane and nuclear regions are denoted. Red fluorescence is observed within cytoplasm (red arrowheads) and nucleus (blue arrowheads) in 4HT treated ROCK:ER but not KD:ER skin.

(C) Pixel intensity of nuclear or total β-catenin staining in 4HT treated KD:ER and ROCK:ER skin sections. Measurements were carried out on 5 fields each of sections derived from three mice per genotype. Western analysis shows β-catenin protein level in pooled epidermal lysates from 4HT treated KD:ER and ROCK:ER mice (3 mice per genotype).

(D) FACS of β-catenin staining versus forward scatter of epidermal cells derived from WT, KD:ER and ROCK:ER skin. Histogram shows percentage β-catenin positive cells in each sample.

(E) Unphosphorylated (Ser37/Thr41)-β-catenin (red) and phosphorylated (Ser9) GSK3β (green) distribution in 4HT treated KD:ER and ROCK:ER skin, either without or with BAPN treatment to inhibit lysyl oxidase.

Figure 5

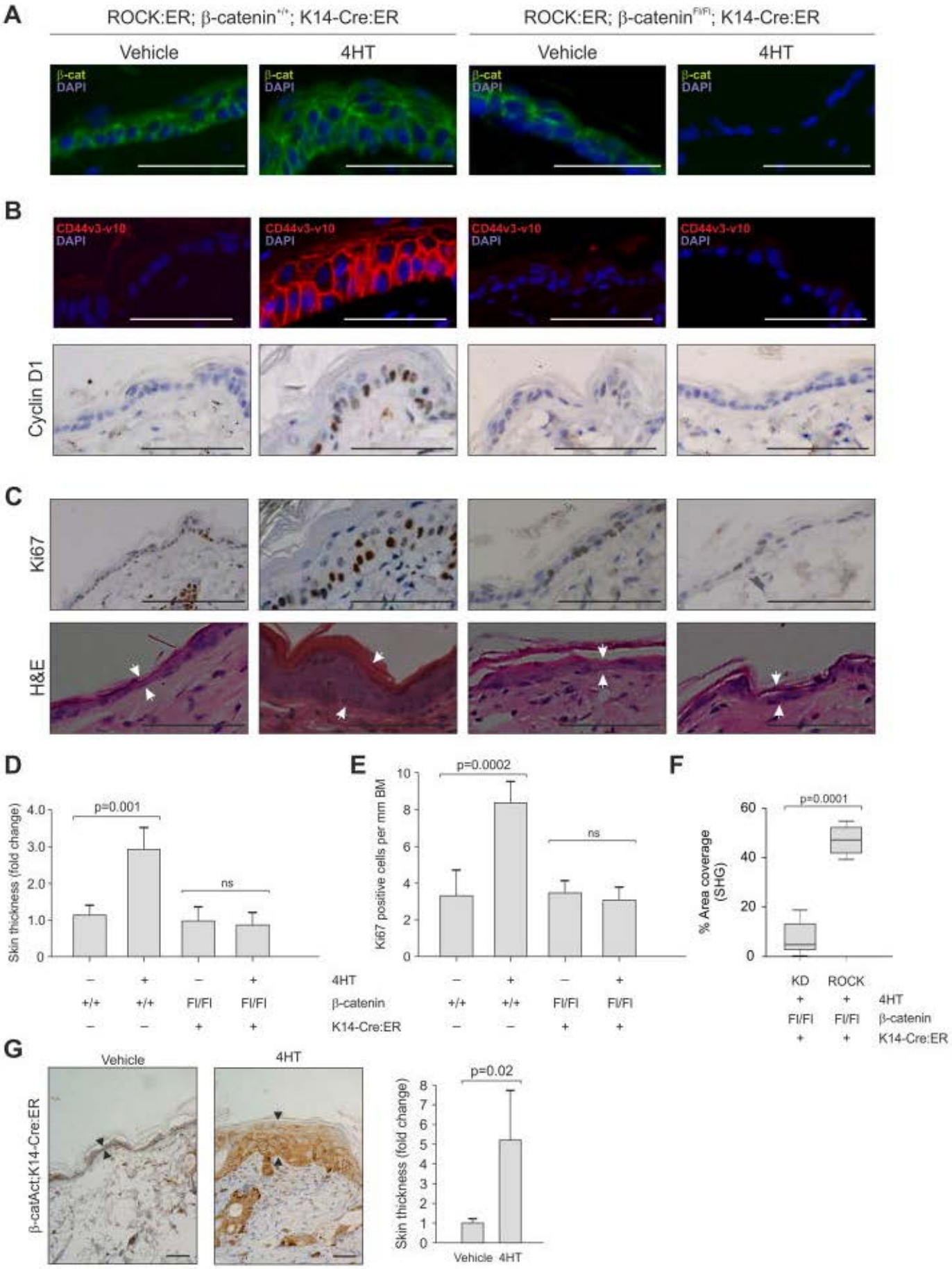

ROCK induced epidermal hyperproliferation is β-catenin dependent

Vehicle or 4HT-treated β-catenin$^{Fl/Fl}$; K14-Cre:ER mice expressing KD:ER or ROCK:ER as indicated were stained or scored for:

(A) β-catenin

(B) β-catenin target genes CD44 (top panels) and Cyclin D1 (bottom panels).

(C) Ki-67 (top panels) and H&E (bottom panels). Skin thickness differences are indicated by white arrow pairs in H&E panels.

(D) Skin thickness

(E) Ki67 positive cells per mm basement membrane

(F) Collagen area coverage by SHG

(G) K14-Cre:ER, Ctnnb1$^{tm1Mmt/+}$ mice were treated as indicated with vehicle or 4HT to activate β-catenin. Panels show β-catenin staining and skin thickness (arrows); histogram indicates fold change in skin thickness.

Scale bars, 100 μm.

See also Figure S4

Figure 6

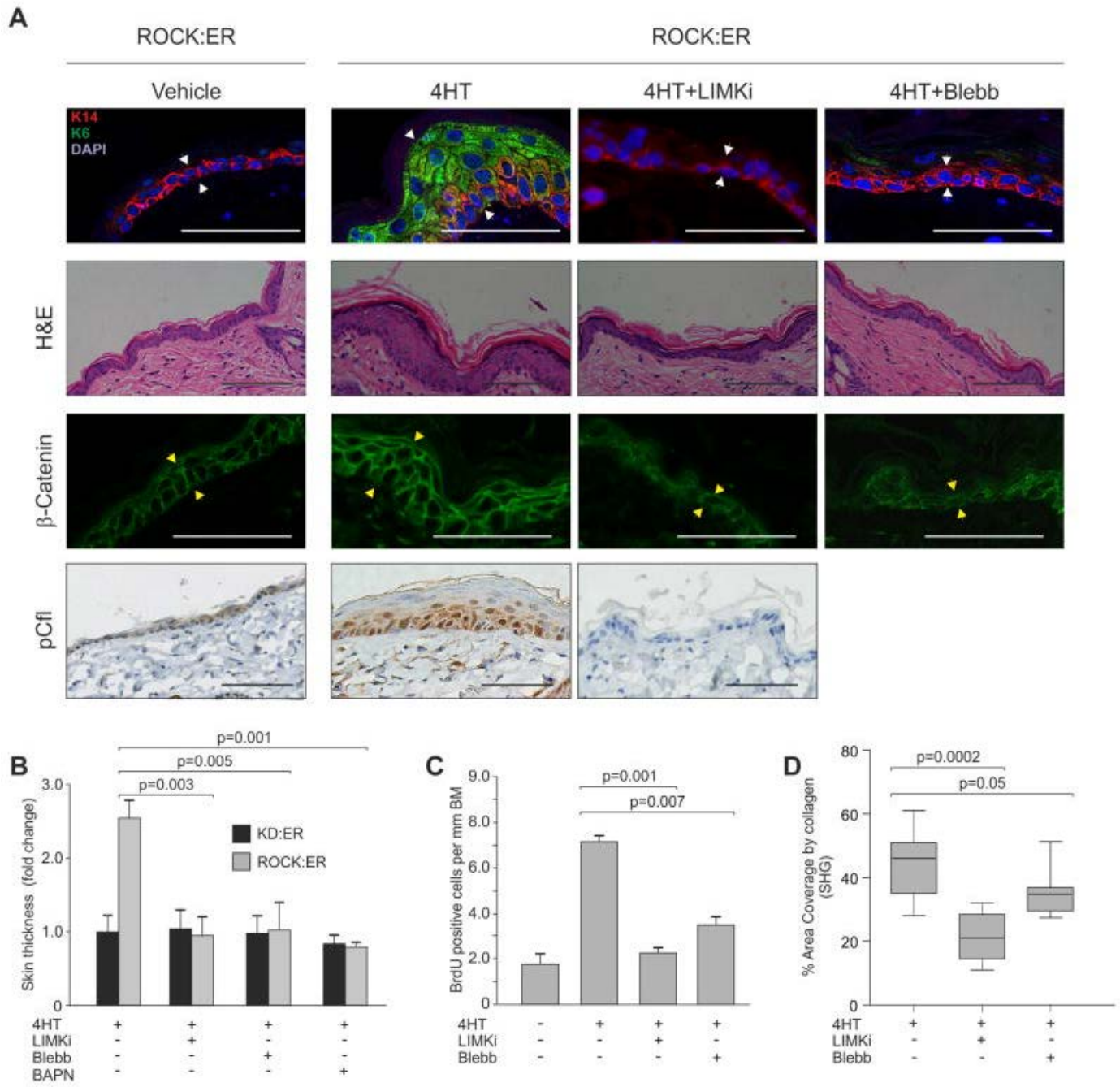

ROCK induced epidermal hyperproliferation is dependent on actomyosin contractility

(A) Skin sections from ROCK:ER mice treated with Vehicle or 4HT, 4HT+LIMKi or 4HT+Blebbistatin, stained with H&E or for K6, K14, β-catenin or pCfl. Scale bars indicate 100 μm.

(B) Fold change in ROCK:ER skin thickness relative to KD:ER skin following 4HT treatment in absence or presence of LIMKi, Blebbistatin or BAPN.

(C) BrdU incorporation scored as positive cells per mm BM from untreated, 4HT-treated 4HT+LIMKi or 4HT+Blebbistatin treated ROCK:ER skin.

(D) Collagen area coverage in ROCK:ER skin following 4HT treatment in absence or presence of LIMKi or Blebbistatin.

See also Figure S5

Figure 7

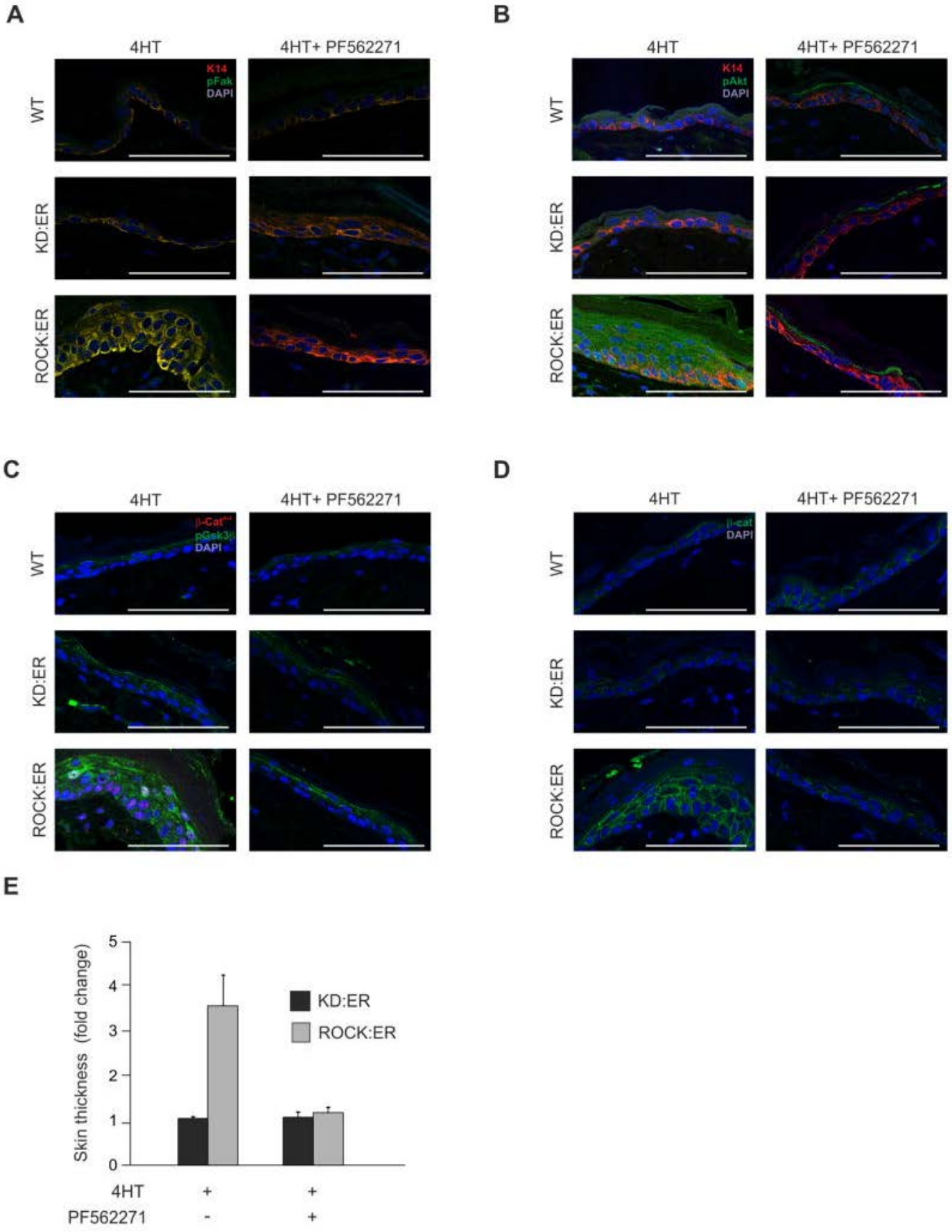

FAK, Akt and GSK3β phosphorylation increased in ROCK-activated skin

WT, KD:ER and ROCK:ER skin treated with 4HT alone or 4HT plus FAK inhibitor PF-562271 stained for:

(A) K14 (red) and FAK pTyr397 (green)

(B) K14 (red) and Akt pSer473 (green)

(C) GSK3β pSer9 (green) and unphosphorylated β-catenin Ser37/Thr41 (red)

(D) Total β-catenin (green)

(E) Fold change in ROCK:ER skin thickness relative to KD:ER skin following 4HT treatment in absence or presence of FAK inhibitor PF-562271.

Scale bars, 100μm

See also Figure S6

Figure 8

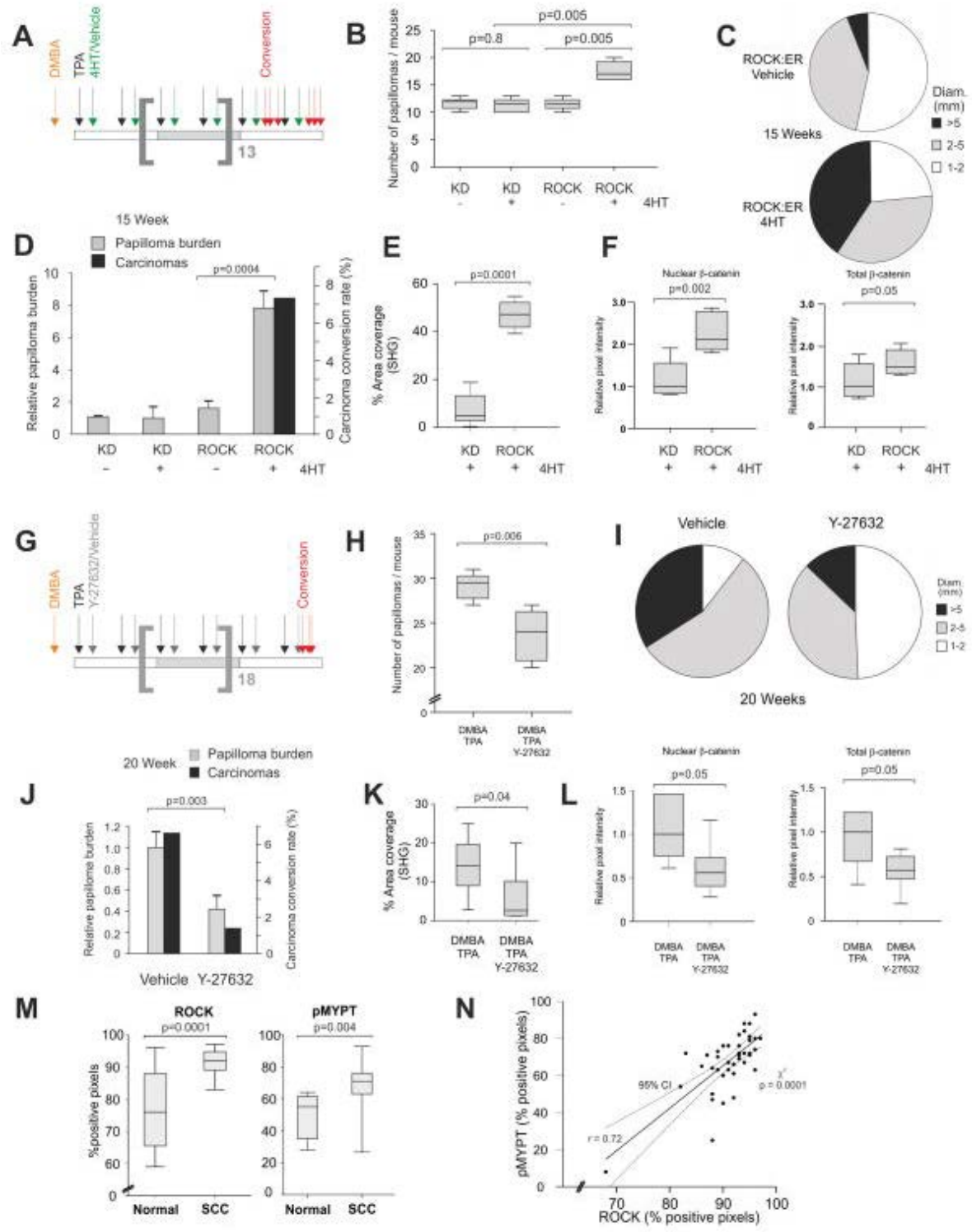

ROCK activation accelerates papilloma growth and progression

(A) Timeline of 15 week chemical carcinogenesis and ROCK activation in cohorts of 6 mice of ROCK:ER and KD:ER genotypes. Treatments were: orange arrow – DMBA, black arrows – TPA, green arrows – 4HT or Vehicle. Papilloma to carcinoma conversions in individual ROCK:ER mice denoted by red arrows.

(B) Box and whisker plot of DMBA/TPA-induced papillomas per mouse in ROCK:ER and KD:ER mice treated with vehicle or 4HT as indicated.

(C) Pie charts of papilloma size distribution at completion of 15 week treatment period in ROCK:ER and KD:ER mice treated with vehicle or 4HT as indicated. Carcinomas are not included.

(D) Histogram of DMBA/TPA papilloma burden and carcinoma conversion rate in ROCK:ER and KD:ER mice treated with vehicle or 4HT as indicated.

(E) Collagen area coverage measured by SHG in 4HT treated KD:ER or ROCK:ER skin.

(F) Pixel intensity of nuclear or total β-catenin staining in 4HT treated KD:ER or ROCK:ER DMBA/TPA papillomas. Measurements were carried out on 7 fields per condition.

(G) Timeline of 20 week chemical carcinogenesis and ROCK inhibition in cohorts of 6 WT FVB/N mice. Treatments were: orange arrow – DMBA, black arrows – TPA, grey arrows – Y27632 or Vehicle. Papilloma to carcinoma conversion events are denoted by red arrows.

(H) Box and whisker plot of DMBA/TPA-induced papillomas per mouse in vehicle or Y27632 treated WT FVB/N mice.

(I) Pie charts of papilloma size distribution at completion of 20 week treatment period in Y27632 or vehicle treated WT FVB/N mice. Carcinomas are not included.

(J) Histogram of DMBA/TPA papilloma burden and carcinoma conversion rate in vehicle or Y27632 treated WT FVB/N mice.

(K) Collagen area coverage measured by SHG in DMBA/TPA treated skin along with vehicle or Y27632.

(L) Pixel intensity of nuclear or total β-catenin staining in vehicle or Y27632 treated DMBA/TPA papillomas. Measurements were carried out on 7 fields per condition.

(M) Results of positive pixel analyses of ROCK expression and MYPT phosphorylation in a sample of 40 human epidermal squamous cell carcinomas.

(N) Correlation curve of pMYPT and ROCK positive pixel analyses. The 95% confidence interval is denoted by dotted lines. Statistical significance was calculated using Chi-square test. A Pearson product-moment correlation coefficient (r) of 0.7 confirms a large correlation between ROCK and pMYPT positive pixels.

See also Table S1